IN-05
13P

NASA Technical Memorandum 109007

Aerothermoelastic Analysis of a NASP Demonstrator Model

J. Heeg, T. A. Zeiler, A. S. Pototzky, C. V. Spain, and W. C. Engelund

October 1993

National Aeronautics and Space Administration

Langley Research Center
Hampton, Virginia 23681-0001

AEROTHERMOELASTIC ANALYSIS OF A NASP DEMONSTRATOR MODEL

Jennifer Heeg*
NASA Langley Research Center
Hampton, Virginia

Thomas A. Zeiler**, Anthony S. Pototzky†, and Charles V. Spain‡
Lockheed Engineering and Sciences Company
Hampton, Virginia

and

Walter C. Engelund§
NASA Langley Research Center
Hampton, Virginia

Abstract

The proposed National AeroSpace Plane (NASP) is designed to travel at speeds up to Mach 25. Because aerodynamic heating during high-speed flight through the atmosphere could destiffen a structure, significant couplings between the elastic and rigid body modes could result in lower flutter speeds and more pronounced aeroelastic response characteristics. These speeds will also generate thermal loads on the structure. The purpose of this research is to develop methodologies applicable to the NASP and to apply them to a representative model to determine its aerothermoelastic characteristics when subjected to these thermal loads. This paper describes an aerothermoelastic analysis of the generic hypersonic vehicle configuration. The steps involved in this analysis were: (1) generating vehicle surface temperatures at the appropriate flight conditions; (2) applying these temperatures to the vehicle's structure to predict changes in the stiffness resulting from material property degradation; (3) predicting the vibration characteristics of the heated structure at the various temperature conditions; (4) performing aerodynamic analyses; and (5) conducting flutter analysis of the heated vehicle. Results of these analyses and conclusions representative of a NASP vehicle are provided in this paper.

Introduction

The National AeroSpace Plane (NASP) vehicle is expected to reach extremely high temperatures as a result of aerothermal heating. The mission profile dictates that the vehicle endure high temperature conditions during ascent and descent. There are large areas of the vehicle that are expected to have little or no thermal protection and may experience large thermal gradients in the structure that could translate into adverse thermal loads. These loads may have an impact on the trim, flutter, limit load, and flight control characteristics of the flight vehicle. Tools have been developed to assess the impact of heating on the vehicle's aeroelastic characteristics. In the course of this development effort, an aeroelastic vehicle representative of the NASP configuration was analyzed for its flutter behavior along the ascent trajectory. The modal and flutter characteristics were compared for the heated and unheated vehicles.

Configuration Description

An unclassified aeroelastic vehicle representative of the NASP configuration and referred to as the demonstrator model was developed for use in this study. A NASP configuration published in Aviation Week[1] served as the basis for this model. A classified model, referred to as the NPO model, provided by the NASP National Project Office provided guidance for modifying the wing and vertical tail planforms and the wing root condition.

The planform and profile of the resulting configuration are shown in figure 1. The vehicle fuselage is 150 feet long and weighs approximately 300,000 lbs fully fueled with a center of gravity at approximately 56 % of the fuselage length. The root leading edge of the all-moveable clipped delta wing begins at 70% fuselage length. The wing has a root chord length of approximately 27% fuselage length, a span of approximately 9.5% fuselage length, a leading edge sweep of 70° and a trailing edge sweep of 15°. The pivot shaft attaches at 65% of the wing root chord. The curved symmetric airfoil is thickest at 65% chord where the thickness is 4% of the local chord. The demonstrator model has twin vertical tails with rudders; the rudder is not modeled structurally. The profile view shows that the forward section of the fuselage acts as a compressor for the airflow as it approaches the engine and the aft portion of the fuselage acts as a nozzle for the engine exhaust.

* Aerospace Engineer, Member AIAA.
** Staff Engineer, Member AIAA.
† Staff Engineer, Senior Member AIAA.
‡ Senior Staff Engineer.
§ Aerospace Engineer, Member AIAA.

Aerothermoelastic Analysis Procedure

Aerothermoelastic analysis of the generic hypersonic vehicle configuration involved the following steps: (1) generating vehicle surface temperatures at the appropriate flight conditions; (2) applying these temperatures to the finite element model (FEM) for predicting changes resulting from material property degradation; (3) predicting vibration characteristics of the heated structure at the various temperature conditions; (4) performing aerodynamic analyses; and (5) conducting flutter analyses of the heated vehicle. For reasons discussed later, the effects of thermal prestress were not included.

Generation of Temperatures

The Hypersonic Arbitrary Body Program contained within the APAS aerodynamic code[2] was used to generate surface temperatures on the vehicle at various flight conditions. Temperatures produced by APAS are a derived from a subroutine used to estimate viscous forces on the vehicle skin. Besides generating local convective heat transfer rates, the code predicts the radiation equilibrium wall temperatures through an iterative process. The aerodynamic paneling used to predict the surface temperatures is shown in figure 2. The temperature distributions are generated at the centers of the aerodynamic panels of the APAS model. For the purpose of making this analysis conservative, it was assumed that the surface temperature was the temperature of the material. Transient heating effects were not included in this analysis because transient thermal modeling was not available and the structural model was not detailed enough to produce an appreciable effect.

Using the APAS code, surface temperature distributions on the vehicle were computed along a typical NASP ascent trajectory. The flight trajectory used for this study is provided in figure 3, along with typical temperature contour plots for three Mach number conditions: 5.0, 15.0, and 25.0. For the vehicle traveling at Mach 5.0, relatively cool temperatures are exhibited. Most of the ramp portion of the vehicle is heated to about 1010° F while the nose area is the hottest at about 1520° F. At Mach 15.0, the surface temperatures are elevated to their highest values with the nose temperature at nearly 5000° F At Mach 25.0, a noticeably cooled vehicle is predicted with respect to the Mach 15.0 case, possibly resulting from flying through a very rarefied atmosphere at an altitude of approximately 50 miles.

Application to Finite Element Model/Vibration Analysis

The methodology developed incorporates the aerodynamic heating effects into the finite element structural model. To accomplish this, an interpolation procedure maps the temperatures, produced by the APAS code, to the finite element node locations and element centers. Additionally, engine heating effects for the Mach 5 through 25 cases have been incorporated. The temperature distributions have been mapped such that the wing leading edge temperatures are averaged values of the forward-most aerodynamic grid points from the top and bottom wing surfaces. An element property interpolator calculates material properties for each element based on the elemental temperatures and material properties tabulated as functions of temperature. Using the new stiffness matrix, vibration analysis is performed on the model.

Unheated Finite Element Model. Engineering Analysis Language[3] was used to generate the structural FEM. The model has 351 gridpoints and is composed mostly of plate/membrane quadrilateral elements and beam elements. The fuselage skins are supported by rings of rigid beams and the wing and fin skins are supported by ribs and spars. This type of modeling produces dynamic behavior representative of a stressed-skin monocoque design while eliminating local or shell modes. The wing pivot shaft has an associated spring stiffness to model the actuator. The symmetric vibration frequencies and mode shapes, shown in figure 4, were obtained by tuning the model mass and stiffness parameters until reasonable agreement with the NPO dynamics model was achieved. Table 1 provides the mode shape labels that have been used to identify the modes.

Material Properties. The material properties of the composites to be used on the NASP were not available for this study. The material properties of titanium-aluminide and carbon-carbon served as the starting point in tuning the unheated model to reflect the NPO model characteristics. The modified material properties then served as the zero-temperature material properties for the model. Trends showing the temperature-dependent material properties of titanium-aluminide and carbon-carbon are shown in figure 5. In applying these properties to the finite element model, they were biased to reflect the previously-modified zero-temperature properties. When heating was included in the modal analysis, the elements in the finite element model were assigned material properties based on the data from figure 5 after biasing and on the nodal temperature. The material properties of titanium-aluminide composed the majority of the structure; the nose of the fuselage and leading edges of the wing and fin were composed of carbon-carbon.

Heating Effects on Vibration Characteristics. Modal analysis was performed for eight heated conditions. The modes, labeled in table 1, remained identifiable as the temperatures increased, even though the modal contributions of portions of the vehicle changed. This is exemplified in figure 6, where the fourth elastic mode is shown for Mach 5, 10, and 20. As the Mach number, and

thus the heating increases, the contribution of the fuselage bending to this mode decreases, the wing pivoting increases and the wing camber decreases. The majority of the natural frequencies of the system decreased when the vehicle was heated as shown in figure 7. The two modes which are relatively unaffected by heating are the wing pivot mode and the wing in-plane mode This is expected since the main drivers for these modal frequencies are the inertia of the wing and the stiffness of the actuator, which remain unchanged.

Aerodynamic Methods and Analysis

The NASP mission requires that the vehicle operate over the entire spectrum of Mach numbers from 0 to 25. Figure 8 shows the aerodynamic theories used in the flutter analyses with respect to Mach number. The doublet lattice method[4] is used for calculations at subsonic Mach numbers and the harmonic gradient method[5] is used for low supersonic Mach numbers. For hypersonic Mach numbers, three different aerodynamic theories were used: van Dyke's second order piston theory[6] for low hypersonic; Newtonian impact theory[7] for high hypersonic; and a blending of these two for the entire hypersonic range. The hypersonic aerodynamic theories will be discussed later.

Shown in figure 9 is the box layout of the half-vehicle used in the aeroelastic modeling for all aerodynamic computations. Factors were applied to the pressures where the boxes did not entirely cover the planform and where they extended beyond the planform. Because of the nature of both doublet lattice and harmonic gradient (low supersonic Mach number) aerodynamic theories, "chordwise" edges of the aerodynamic panels and boxes are required to be streamwise. The rear of the demonstrator model's fuselage fans slightly outward. Thus, the root chord of the wing is not aligned streamwise. The aeroelastic modeling of the wing places the inboard leading edge corner at the proper location, but places the inboard trailing edge corner slightly inboard of its proper location. This produces additional wing area in the model that amounts to approximately 10 percent of the true wing area. Boxes in the additional wing area and on the fuselage adjacent to the additional wing area were given pressure factors as described above.

Unsteady Hypersonic Aerodynamics for Flutter Analysis. Unsteady aerodynamics for vehicles at high supersonic and hypersonic speeds are presently difficult to obtain. There are no commonly available codes that are reliable and accurate and that can be used to obtain unsteady aerodynamics in a routine fashion. At higher Mach number conditions, Van Dyke's second order piston theory can be used to obtain an approximate representation of the aerodynamics. For the van Dyke theory, the pressure coefficient on a surface is

$$C_p = \frac{2}{M\beta}\left[\frac{M}{U}w + \frac{M}{2U^2}\overline{G}w^2\right] \qquad (1)$$

were M is Mach number, U is the airspeed, β is $\sqrt{M^2-1}$, w is the normalwash, and

$$\overline{G} = \frac{M^4(\gamma+1)-4\beta^2}{2\beta^3}.$$

γ is the ratio of specific heats. The unsteady normalwash is given by

$$w = \frac{\partial Z}{\partial \tau} + U\frac{\partial Z}{\partial x} \qquad (2)$$

which includes contributions from both the normal motion of the surface Z and its inclination to the flow. In general, the vibration modes, thickness and camber slopes, and angle of attack would all contribute to the normalwash. However, once the pressures for both the upper and lower surfaces are differenced, the camber and angle of attack contributions vanish in the modal terms. The equation for the total lifting pressure is linearized in the vibration mode generalized coordinates giving, for the ith mode, ϕ_i,

$$\Delta C_p(k) = -\frac{4}{\beta}\left(1 + \frac{\overline{G}}{2}\frac{\partial t}{\partial x}\right)\left[\frac{\partial \phi_i}{\partial x} + j\frac{k}{b_r}\phi_i\right] \qquad (3)$$

which includes both the variation in thickness, t, and the unsteady motion (k is reduced frequency and b_r is the reference semichord).

At high Mach number and flow incidence angles where van Dyke theory is not applicable, Newtonian impact theory[7] can be used. Newtonian impact theory gives the pressure coefficient as

$$C_p = C_{p_{max}} \sin^2\theta \qquad (4)$$

where θ is the total angle between the flow direction and the local surface inclination and

$$C_{p_{max}} = \frac{2}{\gamma M^2}\left\{\left[\frac{(\gamma+1)^2M^2}{4\gamma M^2 - 2(\gamma-1)}\right]^{\frac{\gamma}{\gamma-1}}\left[\frac{1-\gamma+2\gamma M^2}{\gamma+1}\right]\right\} \qquad (5)$$

Another feature of Newtonian impact theory is the shadowing effect wherein pressure coefficients on leeward surfaces are set to zero or near zero. As in the van Dyke theory, the total angle includes vibration mode deformation

as well as motion, the camber and thickness variation, and the angle of attack. When the pressure coefficient is linearized in the vibration mode generalized coordinates, the coefficients of the vibration mode terms contain contributions from angle of attack, and camber and thickness variation. The total incidence, excluding the flexible contribution, is used to determine whether or not the point in question is on a leeward surface. However, if all of the non-flexible incidences are zero, then the coefficients of the vibration mode terms are zero. The undesirable result would be that the vibratory motion produces no pressures.

Clearly, Newtonian impact theory is best used for flow conditions where there is a combination of high Mach number and high flow incidence. Since this flow condition is not present everywhere on a body, a rational blending of the van Dyke and Newtonian theories is more desirable. Thus, when pressure coefficients on individual aerodynamic boxes are calculated, a comparison is made between the local flow incidence or deflection angle and the shock angle associated with that flow deflection angle. The shock angle is easily solved for by iterating on the well-known oblique shock relations[8]. These angles are depicted in figure 10. If the angle is greater than some predefined test angle, the van Dyke pressure coefficient is applied to the aerodynamic box in question. If the shock angle is between this test angle and the minimum possible shock angle that occurs for infinite Mach number, a weighted average of the van Dyke and Newtonian impact pressure coefficients is used. The weighting is determined by

$$w = \frac{\beta_{test} - \beta}{\beta_{test} - \beta_{min}} \qquad (6)$$

and the pressure coefficients are weighted according to

$$C_p = (1 - w)C_{pVD} + wC_{pNI} \qquad (7)$$

For the analyses presented in this paper, the test shock angle was defined as 4/3 the minimum shock angle. Between Mach numbers 5.0 and 10.0, the shadowing effect is linearly varied from no shadowing at Mach 5.0 to full shadowing at Mach 10.0 and above. Since flow conditions may be different between upper and lower surfaces, the blending and shadowing variation require that the van Dyke pressure coefficients on upper and lower surfaces be calculated separately before they are combined into the net lifting pressure coefficient. This is different from assuming van Dyke aerodynamics alone, for which equation 3 is used.

As will be seen in the flutter results, the blending procedure produces flutter boundaries that are continuous throughout the Mach range and display the character of both unblended approaches at extreme ends of the Mach number range. These characteristics of the blended approach do not fully justify its use. It is felt, however, that this approach is at least as sound as using either van Dyke or Newtonian impact theory alone. There is obviously much work to be done in the area of linear hypersonic aerodynamic theories suitable for aeroelastic calculations.

Aeroelastic Analysis

Modal characteristics were obtained from a finite element model of the vehicle. Nine modes are used in the symmetric analyses: rigid body plunge and pitch and seven free-body elastic modes. Ten modes were used in the antisymmetric analyses: rigid body side motion, roll, and yaw and seven elastic modes.

Match point flutter analyses were performed for Mach numbers ranging from 0.2 to 25.0 using the AVA (Aeroelastic Vehicle Analysis) system of computer codes[9]. Analyses were performed for nine symmetric modes, both unheated and heated, obtained from the finite element model described earlier. The nine modes were: rigid body plunge and pitch; and seven free-body elastic modes. Structural damping of 3% was assumed to exist for all elastic modes and an angle of attack of 2 degrees was assumed for the hypersonic calculations. Analysis results are displayed as stability boundaries plotted as equivalent airspeed versus Mach number, with lines of constant altitude included. Also displayed is a typical ascent trajectory.

Symmetric Unheated Case. Figure 11 shows stability boundaries up to Mach 10 without effects on the flexible modes. At subsonic Mach numbers, there is a region of short period mode instability at low frequency, which may indicate longitudinal static instability. This instability restabilizes at higher dynamic pressures, probably as a result of the wing aeroelastically washing-in, thus providing a greater pitch restoring moment. The instability also disappears as transonic Mach numbers are approached. Since the doublet lattice method is not suitable for transonic calculations, it is uncertain how realistic this trend is. At higher dynamic pressures, a body freedom flutter mode appears. This flutter mode occurs as the frequencies of the short period mode and the second elastic mode coalesce. The second elastic mode is the wing pivot mode, which aeroelastically washes-in. Thus, its frequency drops with increasing dynamic pressure as the short period mode frequency rises. This body freedom flutter mode is similar to the body freedom flutter mode to which forward swept wing aircraft are susceptible[9].

At low supersonic Mach numbers, where the harmonic gradient method is applied, the vehicle again exhibits a low frequency short period mode instability that restabilizes at higher dynamic pressures and higher Mach numbers. As dynamic pressure increases, body freedom flutter again occurs. There is an additional, "elastic" flutter mode that

does not occur subsonically. This flutter mode occurs when the wing pivot mode's frequency drops to coalesce with the frequency of the fuselage first bending mode. A root locus plot for a Mach number of 3.0 and density for 20,000 feet altitude (standard atmosphere), using harmonic gradient aerodynamics, is shown in figure 12a. Note that only one point along any eigenvalue trace is a matched point. This plot shows how the frequencies of the aeroelastic modes change as airspeed is increased. Since thickness effects become more important as Mach number increases, the flat plate analysis used at the lower supersonic Mach numbers is no longer applicable in the hypersonic region. The hypersonic analyses show the low frequency short period mode instability and the body freedom flutter mode. They also show the elastic flutter mode occurring between the short period restabilization and the body freedom flutter mode. A root locus plot for a Mach number of 5.0 and density for 45,000 feet altitude, using blended van Dyke/Newtonian impact aerodynamics, is shown in figure 12b. Note from figures 11 and 12b that the elastic flutter mode is a hump mode that restabilizes at a higher dynamic pressure. Note also that, as hypersonic Mach number increases further, the only instability is the low frequency short period mode instability.

Symmetric, Heated Case. As was mentioned earlier in this paper, only the effects of heating on material properties were considered in this study. Figure 13 shows the symmetric aeroelastic stability boundaries for the heated vehicle. Mode shapes for the heated vehicle were not obtained for Mach numbers below 5.0 so only hypersonic results are shown. With the heating effects are included, the short period mode instability does not restabilize. As a consequence, body freedom flutter does not occur. The elastic mode flutter occurs as a hump mode and remains throughout a greater Mach number range than for the unheated vehicle. Further, the heating effects lower the boundary of the elastic mode flutter, but not down to the trajectory curve. The unheated result is shown on this figure for comparison.

Below Mach 10, there was little difference between the stability boundaries predicted with van Dyke aerodynamics alone and those predicted using the blended van Dyke/Newtonian impact aerodynamics; only the latter is indicated in the figure. Also shown on the figure is the stability boundary predicted using Newtonian impact theory alone above Mach 10. The discontinuous stability boundaries, mentioned earlier, that result from using the two hypersonic aerodynamic theories without blending is evident in the figure.

Issues and Recommendations

The results presented here are for a NASP demonstrator model. This model was designed to have the same modal characteristics as the NPO configuration, without being a classified model. As such, it is felt that the methods and procedures are applicable to the actual NASP vehicle, and the results are representative of the types of problems that may be encountered by this class of vehicle. The following discussions explore assumptions that were made and the validity and impact of each.

Heating changes the stiffness characteristics of the structure in two ways. First, the properties of a heated material differ from its room temperature properties. Second, when constrained structural components expand, internal stresses result (prestressing effect). Initial studies done on the NASP demonstrator model, generated two sets of stiffness data One set incorporated the influence of the material property changes and the other incorporated this influence as well as prestressing. Analysis of the prestressed model indicated that even for very low stress levels, buckling occurred. The current finite element structural model is a dynamics model, lacking the fidelity required for analysis of the prestress effects. It contains no buckle-resistant hat-stiffened panels, stress relief connections or buckle-resistant internal structure. Therefore, the analyses incorporating the prestress effect were discontinued. Past research has shown that the prestress can have a significant impact on the flutter characteristics of a vehicle[10]. These effects can be adverse or propitious, sensitive to changes in the heating condition or material properties.

The mass of the fuel is a significant fraction of the total vehicle mass. As such, it is necessary to model the fuel loading for a specific flight condition in the structural model. For each flutter point examined, a separate finite element model should be generated. For this study, the fuel loading was held constant at the take-off condition.

The material properties used in this study were the best unclassified data obtainable. The room temperature values were based on tuning the frequencies to match to the NPO model. Furthermore, the variations with temperature are for certain materials, not necessarily the materials that are still under consideration for the NASP vehicle.

Performing an accurate aerothermoelastic analysis of a flight vehicle requires remedying these issues.

Conclusions

Aerothermal loads have been shown to have an impact on the aeroelastic characteristics of a NASP-like configuration. As heat loads were applied, the material property degradations lead to modification of the vehicle's modal and flutter characteristics. Three flutter mechanisms were identified for the unheated demonstrator model; all three were influenced by the inclusion of aerothermal loads.

Aerothermal loads caused the short period mode to remain unstable throughout the flight envelope analyzed. Consequently, the body freedom flutter mode, which was present for the unheated vehicle, does not occur for the heated vehicle. Elastic mode flutter, which was present for the unheated vehicle only over a very small Mach number range, is present over a much larger Mach range for the heated vehicle, and occurs at a lower speed.

Tools and methodologies were developed to assess the impact of heating on the vehicle's aeroelastic characteristics. A steady aerodynamic code produced the temperature distributions; a material property interpolation code then calculated the properties for each of the elevated-temperature elements. A system of computer codes was developed to compute the aerodynamics and performed the aeroelastic analysis. An important element of this tool was an aerodynamic method that combined two established hypersonic theories used in flutter analysis.

References

1. Kandebo, S.: Lifting Body Design is Key to Single-Stage-to-Orbit. Aviation Week & Space Technology, McGraw-Hill Publication, October 29, 1990.

2. Divan, P.: Aerodynamic Preliminary Analysis System II, Part II Users Manual, NASA CR-165628, 1981.

3. Whetstone, W.: EISI-EAL Engineering Analysis Language Reference Manual, Engineering Information Systems, Inc., San Jose, CA, 1983.

4. Giesing, J.; Kalman, T.; and Rodden, W.: Subsonic Unsteady Aerodynamics for General Configurations, Part I, Direct Application of the Nonplanar Doublet-Lattice Method, AFFDL-5 Volume I, November 1971.

5. Liu, D.; James, D.; Chen, P.; and Pototzky, A.: Further Studies of Harmonic Gradient Method for Supersonic Aeroelastic Applications, AIAA Journal of Aircraft, Vol. 28, No. 9, pp. 598-605, September 1991.

6. Morgan, H.; Huckel, V.; and Runyan, H.: Procedure for Calculating Flutter at High Hypersonic Speed Including Camber Deflection, and Comparison with Experimental Results. NACA TN-4335, September 1958.

7. Yates, E. C.; and Bennett, R. M.: Analysis of Supersonic-Hypersonic Flutter of Lifting Surfaces at Angle of Attack. AIAA Paper No. 71-327, presented at the AIAA 12th Structures, Structural Dynamics, and Materials Conference, April 1971.

8. Ames Research Staff: Equations, Tables, and Charts for Compressible Flow, NACA 1135, 1953.

9. Weisshaar, T. A..; Zeiler, T. A.; Hertz, T. J.; and Shirk, M. H.: Flutter of Forward Swept Wings, Analyses and Tests. AIAA Paper No. 82-0646, presented at the AIAA 23rd Structures, Structural Dynamics, and Materials Conference, May 1982.

10. Spain, C. V.; Soistmann, D. L.; and Linville, T. W.: Integration of Thermal Effects Into Finite Element Aerothermoelastic Analysis With Illustrative Results, NASP CR-1059, August 1989.

Table 1. Identities for the unheated vehicle symmetric modes.

Flexible Mode Number	Frequency (Hz)	Mode Identity
1	2.95	Fuselage first bending
2	3.85	Wing pivot
3	5.53	Wing in-plane
4	5.72	Fuselage second bending, wing pivot and camber
5	7.74	Wing camber, fuselage third bending (out of phase)
6	8.86	Wing camber and pivot, fuselage third bending (in phase)
7	10.95	Fuselage fourth bending

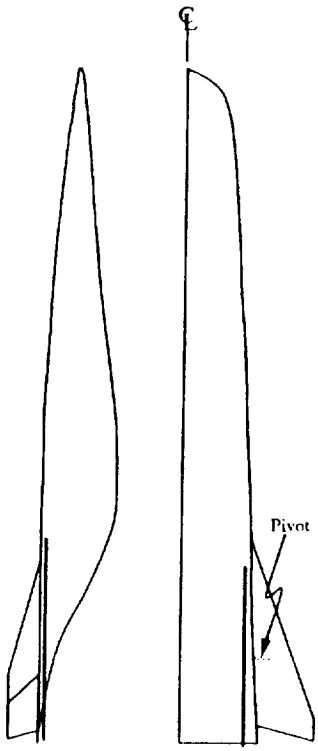

Fig. 1. Profile/planform of NASP demonstrator model.

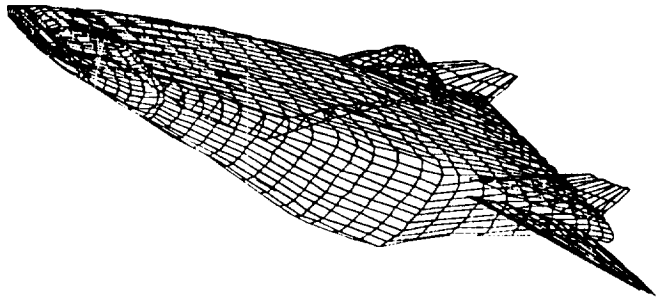

Fig. 2. APAS aerodynamic paneling.

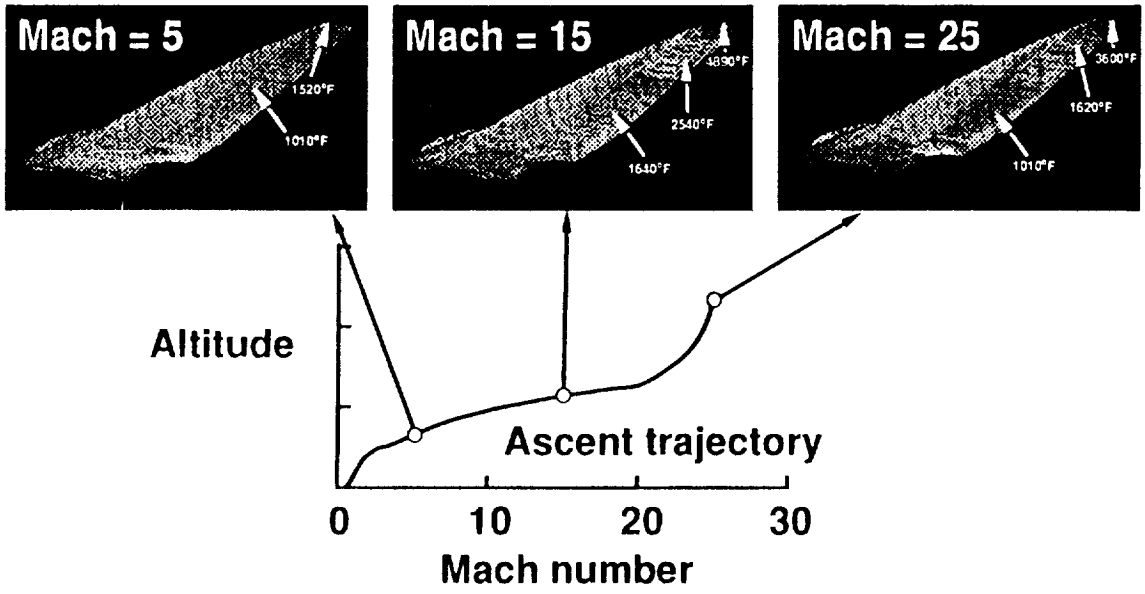

Fig. 3. Temperature distributions predicted by APAS on an ascent trajectory.

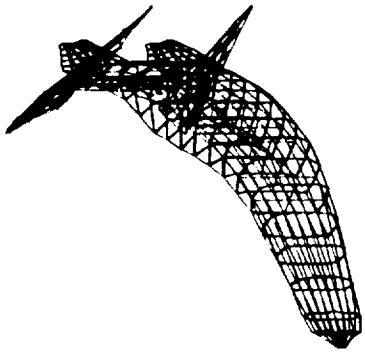

a. 1st elastic mode, 2.95 Hz

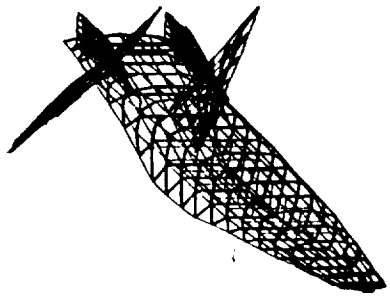

b. 2nd elastic mode, 3.85 Hz

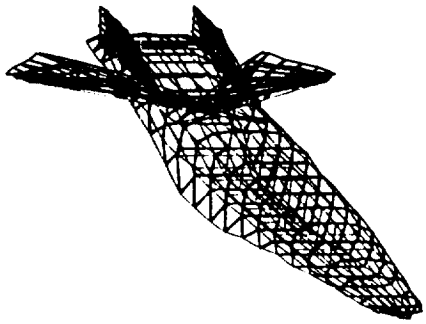

c. 3rd elastic mode, 5.53 Hz

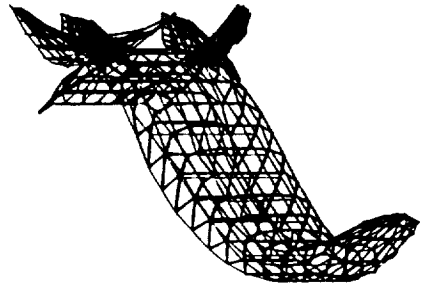

d. 4th elastic mode, 5.72 Hz

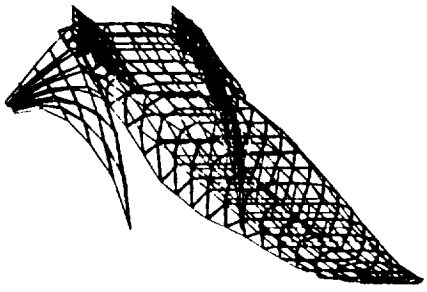

e. 5th elastic mode, 7.14 Hz

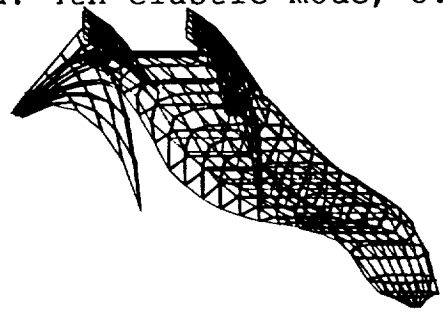

f. 6th elastic mode, 8.86 Hz

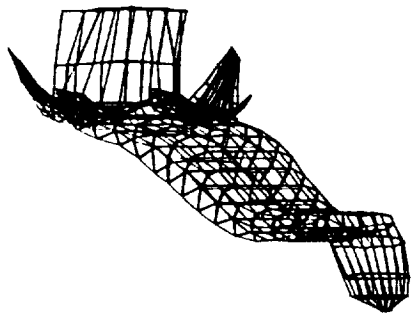

g. 7th elastic mode, 10.94 Hz

Fig. 4. Unheated vehicle elastic modes of generic NASP configuration.

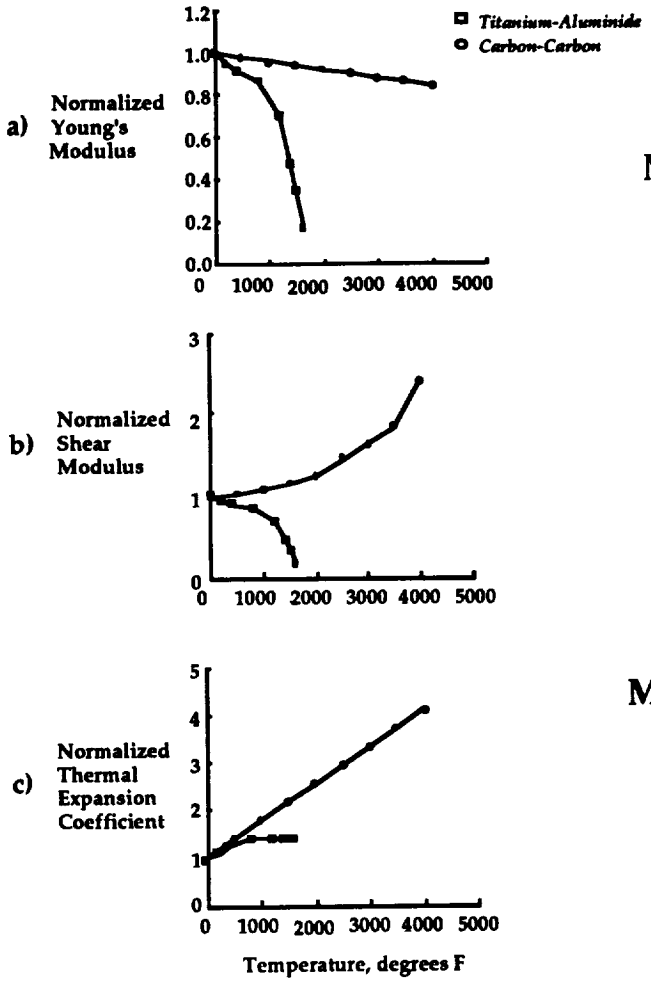

Fig. 5. Material property variations with temperature.

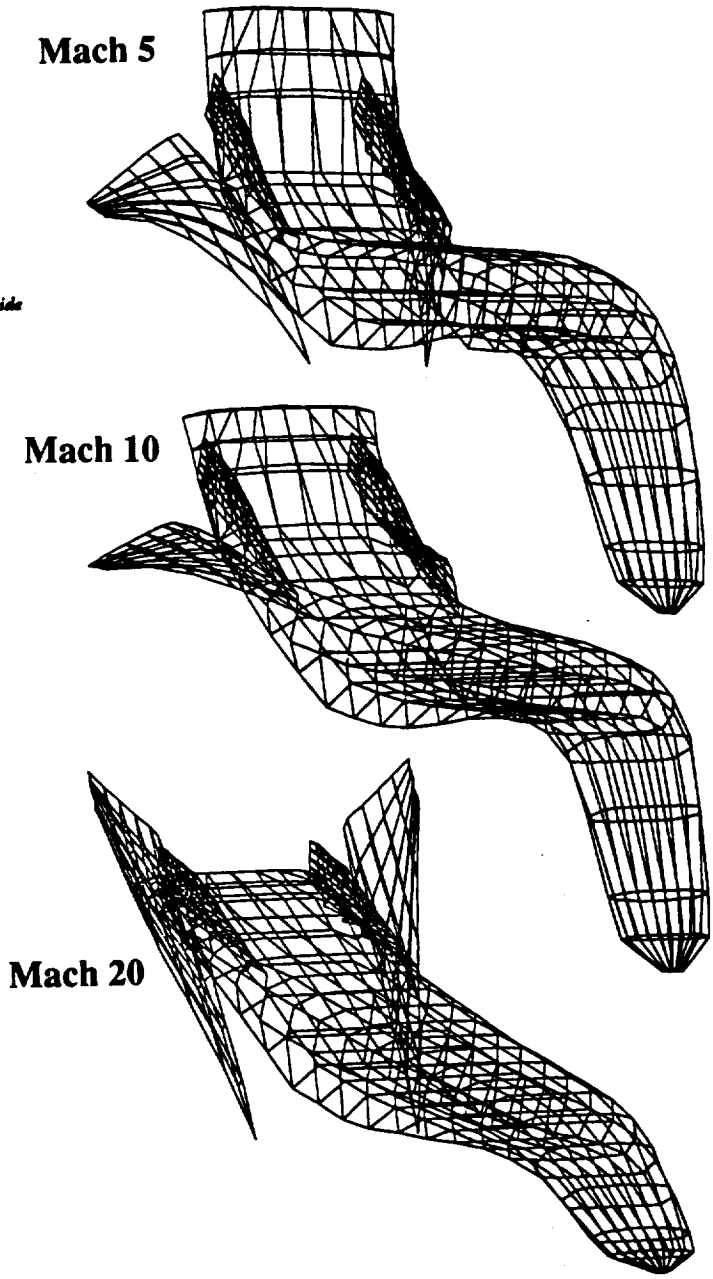

Fig. 6. Variation of the fourth symmetric elastic mode due to heating from Mach 5 to 20.

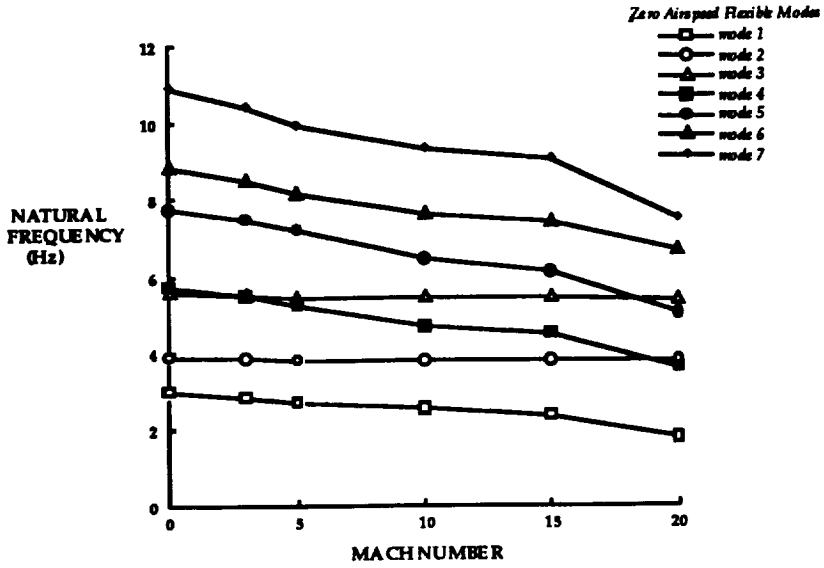

Fig. 7. Heating effects on undamped natural frequencies corresponding to Mach number.

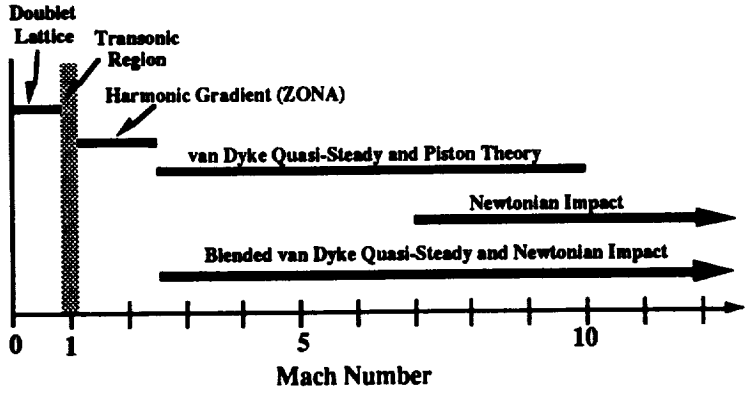

Fig. 8. Aerodynamic theories used for flutter calculations.

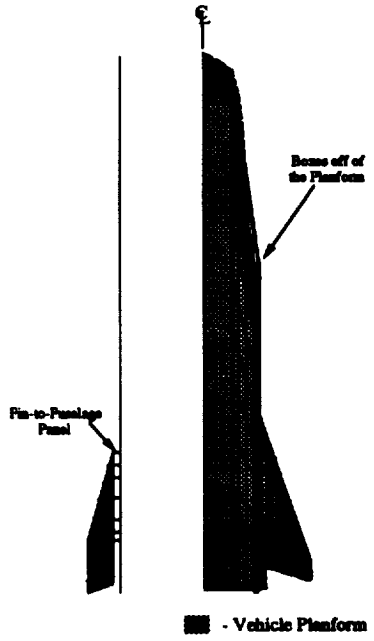

Fig. 9. Aeroelastic box layout of NASP demonstrator model.

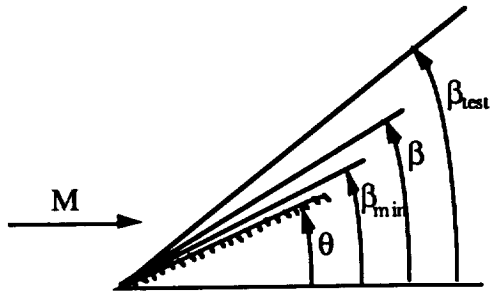

θ Flow deflection angle

β Actual shock angle

β_{min} Minimum possible (infinite M) shock angle

β_{test} van Dyke limit shock angle $= f\,\beta_{min}$

Fig. 10. Shock angles for van Dyke/Newtonian impact blending technique.

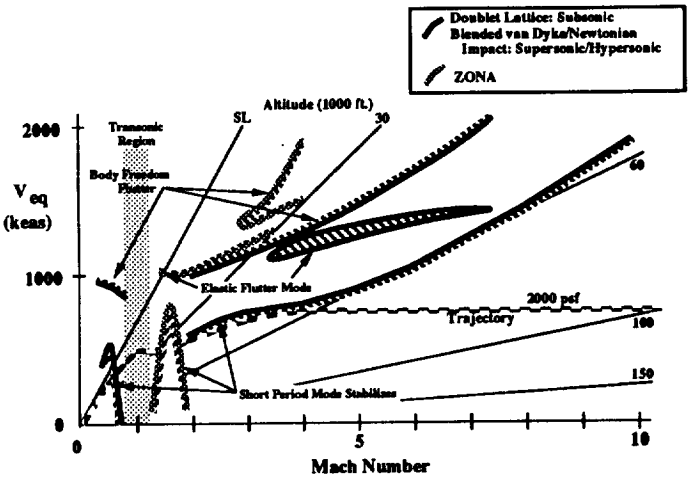

Fig. 11. Symmetric aeroelastic stability boundaries for unheated demonstrator model.

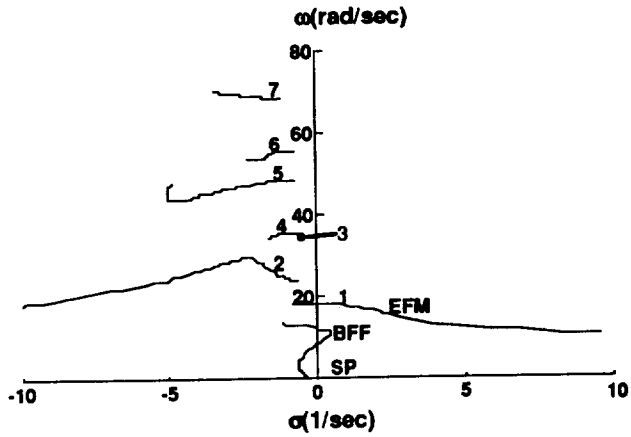

Fig. 12a) Root locus for demonstrator model using ZONA51C aerodynamics at Mach 3.0 and altitude of 20,000 ft.

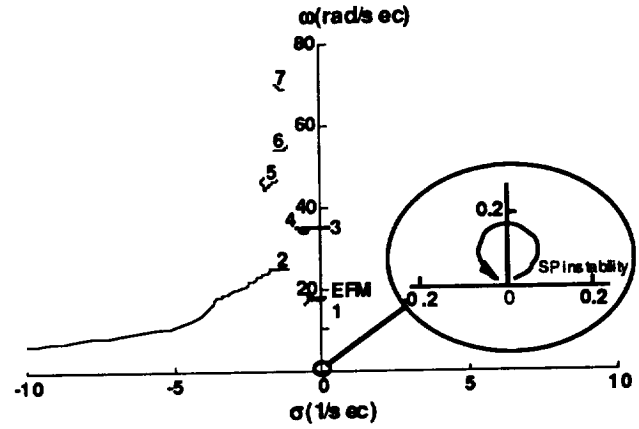

Fig. 12b) Root locus for demonstrator model using blended aerodynamics at Mach 5.0 and altitude of 45,000 ft.

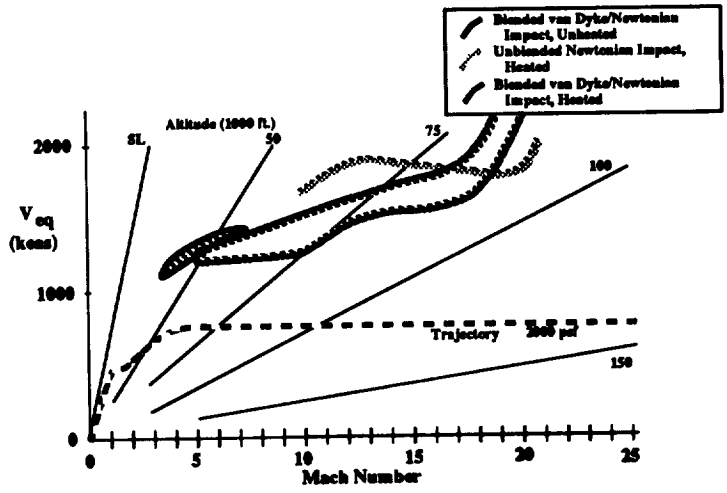

Fig. 13. Effects of heating and hypersonic modeling on symmetric aeroelastic stability boundaries for demonstrator model.

REPORT DOCUMENTATION PAGE

Form Approved
OMB No 0704-0188

1. AGENCY USE ONLY (Leave blank)	2. REPORT DATE	3. REPORT TYPE AND DATES COVERED
	October 1993	Technical Memorandum

4. TITLE AND SUBTITLE
Aerothermoelastic Analysis of a NASP Demonstrator Model

5. FUNDING NUMBERS
WU 505-63-50-15

6. AUTHOR(S)
J. Heeg, T. A. Zeiler, A. S. Pototzky, C. V. Spain, and
W. C. Engelund

7. PERFORMING ORGANIZATION NAME(S) AND ADDRESS(ES)
NASA Langley Research Center
Hampton, VA 23681-0001

8. PERFORMING ORGANIZATION REPORT NUMBER

9. SPONSORING / MONITORING AGENCY NAME(S) AND ADDRESS(ES)
National Aeronautics and Space Administration
Washington, DC 20546-0001

10. SPONSORING / MONITORING AGENCY REPORT NUMBER
NASA TM-109007

11. SUPPLEMENTARY NOTES
Presented at the AIAA 34th Structures, Structural Dynamics, and Materials Conference, 4/19-21/93, LaJolla, CA. Heeg and Engelund: NASA Langley Research Center, Hampton, VA; Zeiler, Pototzky, and Spain: Lockheed Engineering and Sciences, Co., Hampton, VA.

12a. DISTRIBUTION / AVAILABILITY STATEMENT
Unclassified - Unlimited

Subject Category 05

12b. DISTRIBUTION CODE

13. ABSTRACT *(Maximum 200 words)*

The proposed National AeroSpace Plane (NASP) is designed to travel at speeds up to Mach 25. Because aerodynamic heating during high-speed flight through the atmosphere could destiffen a structure, significant couplings between the elastic and rigid body modes could result in lower flutter speeds and more pronounced aeroelastic response characteristics. These speeds will also generate thermal loads on the structure. The purpose of this research is to develop methodologies applicable to the NASP and to apply them to a representative model to determine its aerothermoelastic characteristics when subjected to these thermal loads. This paper describes an aerothermoelastic analysis of the generic hypersonic vehicle configuration. The steps involved in this analysis were: (1) generating vehicle surface temperatures at the appropriate flight conditions; (2) applying these temperatures to the vehicle's structure to predict changes in the stiffness resulting from material property degradation; (3) predicting the vibration characteristics of the heated structure at the various temperature conditions; (4) performing aerodynamic analyses; and (5) conducting flutter analysis of the heated vehicle. Results of these analyses and conclusions representative of a NASP vehicle are provided in this paper.

14. SUBJECT TERMS
Aerothermal, National AeroSpace Plane,
aeroservothermoelasticity, aeroelasticity

15. NUMBER OF PAGES
12

16. PRICE CODE
A03

17. SECURITY CLASSIFICATION OF REPORT	18. SECURITY CLASSIFICATION OF THIS PAGE	19. SECURITY CLASSIFICATION OF ABSTRACT	20. LIMITATION OF ABSTRACT
Unclassified	Unclassified		